Nuclear Engineering and Technology 53 (2021) 3196–3206

Contents lists available at ScienceDirect

Nuclear Engineering and Technology

journal homepage: www.elsevier.com/locate/net

Original Article

Implementation of a new empirical model of steam condensation for the passive containment cooling system into MARS-KS code: Application to containment transient analysis

Yeon-Gun Lee [a, *], Sang Gyu Lim [b]

[a] Department of Nuclear and Energy Engineering, Jeju National University, 102 Jejudaehak-ro, Jeju-si, Jeju, 63243, Republic of Korea
[b] Korea Hydro and Nuclear Power - Central Research Institute, 70 Gil, Yuseong-daero 1312, Yuseong-gu, Daejeon, 34101, Republic of Korea

ARTICLE INFO

Article history:
Received 31 December 2020
Received in revised form
3 April 2021
Accepted 25 April 2021
Available online 2 May 2021

Keywords:
Passive containment cooling system
Steam condensation
Empirical correlation
MARS-KS code
Containment transient

ABSTRACT

For the Korean design of the PCCS (passive containment cooling system) in an innovative PWR, the overall thermal resistance around a condenser tube is dominated by the heat transfer coefficient of steam condensation on the exterior surface. It has been reported, however, that the calculated heat transfer coefficients by thermal-hydraulic system codes were much lower than measured data in separate effect tests. In this study, a new empirical model of steam condensation in the presence of a noncondensable gas was implemented into the MARS-KS 1.4 code to replace the conventional Colburn-Hougen model. The selected correlation had been developed from condensation test data obtained at the JERICHO (JNU Experimental Rig for Investigation of Condensation Heat transfer On tube) facility, and considered the effect of the Grashof number for naturally circulating gas mixture and the curvature of the condenser tube. The modified MARS-KS code was applied to simulate the transient response of the containment equipped with the PCCS to the large-break loss-of-coolant accident. The heat removal performances of the PCCS and corresponding evolution of the containment pressure were compared to those calculated via the original model. Various thermal-hydraulic parameters associated with the natural circulation operation through the heat transport circuit were also investigated.

1. Introduction

Many design concepts of future light water reactors (LWRs) have adopted a passive cooling strategy of the containment via heat removal of steam condensation maintained by natural driving forces. Unlike the PCCS of AP1000 [1] or the Containment Cooling Condenser of KERENA [2], the Korean design of the PCCS in an innovative LWR, named iPOWER, chose an internal condenser type as illustrated in Fig. 1 [3]. That is, it consists of tubular heat exchanger assemblies arranged vertically inside the containment. In the event of a postulated accident followed by violent release of steam into the containment, the steam mixed with the air condenses on the exterior side of condenser tubes. The heat transferred through the tube wall drives a naturally circulating flow of cooling water in the open loop to transport the decay heat from the core to the ultimate heat sink outside of the containment. The inevitable presence of a noncondensable gas inside the containment complicates the condensation phenomena associated with the PCCS. Since a noncondensable gas degrades dramatically the rate of heat transfer by steam condensation, the overall thermal resistance around a condenser tube is dominated by the heat transfer coefficient on the exterior surface in contact with the air-steam mixture.

Not relying essentially on containment analysis codes, the transient behavior of the containment equipped with the PCCS can be investigated with thermal-hydraulic system codes, which were proved generally to provide high-fidelity predictions on two-phase natural circulation flows [4–7]. Among various system codes, Korean nuclear authorities utilize the MARS-KS code for safety analysis of domestic nuclear power plants [8]. In this code, the heat flux by steam condensation in the presence of a noncondensable gas is calculated by Colburn-Hougen model [9], which is a mechanistic model based on the diffusion theory. This model calculates the mass transfer coefficient by using the heat and mass transfer analogy, and thus its accuracy depends on the empirical correlation selected for each flow pattern, i.e. laminar, turbulent, or natural convection flow. Note that it has been found the coded model in the

* Corresponding author.
E-mail address: yeongun2@jejunu.ac.kr (Y.-G. Lee).

https://doi.org/10.1016/j.net.2021.04.024

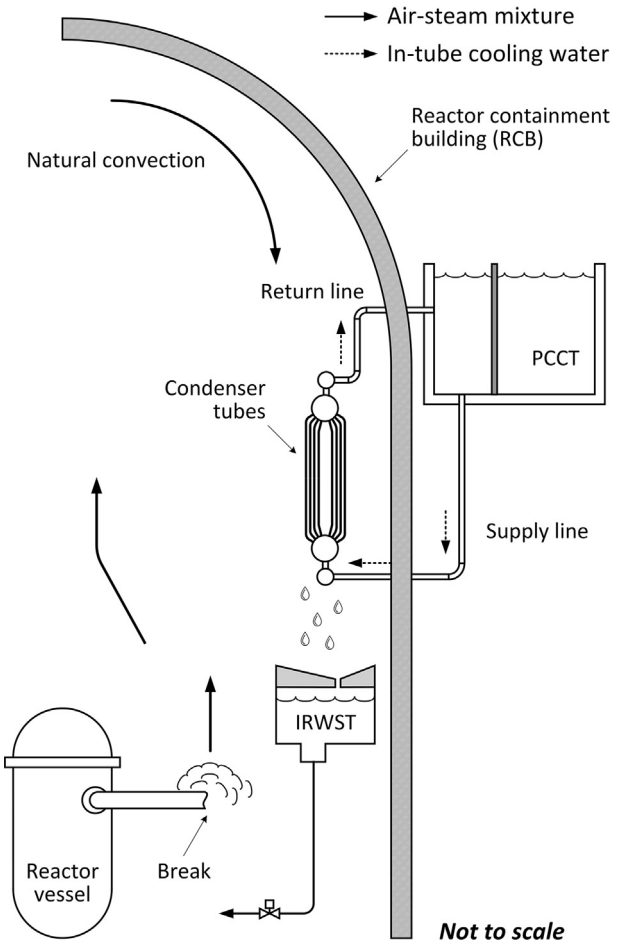

Fig. 1. Illustration of the PCCS to be deployed inside the containment of iPOWER [3].

MARS-KS code had a trivial error in calculating the condensation mass flux, and the source code was corrected to account properly for the effect of a noncondensable gas [10].

Our preliminary study has found, however, that even the corrected code underestimated substantially the condensation heat transfer coefficient on a vertical cylinder in the presence of a noncondensable gas [11]. We had simulated condensation tests performed at Massachusetts Institute of Technology (MIT) with the MARS-KS code. In the test, the heat transfer coefficient was measured on a very long cylindrical tube of 38 mm in outer diameter and 3.5 m in length [12]. Fig. 2 shows the comparison results between calculated heat transfer coefficients and experimental data obtained at 1.5 atm and 3.0 atm. It was revealed that the embedded condensation model in the MARS-KS code substantially underestimated the heat transfer coefficient; then the heat removal rate of the PCCS will be underpredicted with this model. This may mislead the design decision as if the PCCS requires a larger heat transfer area of heat exchangers than it actually would in order to satisfy the design criteria. If one considers the fact that normal containment buildings have a limited free space in which the PCCS can be installed, to place more number of condenser tubes or to deploy longer condenser tubes than needed is not desirable. For the best-estimate prediction of heat removal performance of the PCCS, it is required to replace the embedded condensation model (Colburn-Hougen model) in the system analysis code with an alternative one validated against sufficient number of dataset from separate effect tests.

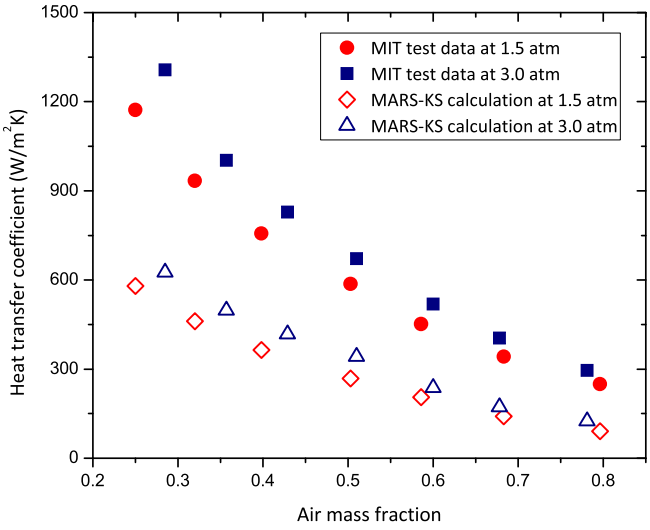

Fig. 2. Results of the preliminary analysis on MIT condensation tests with the MARS-KS code [11].

In this study, we implemented a new empirical correlation of steam condensation in the presence of a noncondensable gas into the MARS-KS version 1.4, which had been developed from condensation test data obtained in the JERICHO facility at Jeju National University (JNU) [13,14]. MIT tests and JNU tests were simulated using the MARS-KS code with the new correlation to evaluate the adequacy of the implemented model. The modified MARS-KS code was applied to simulation of the transient response of the containment equipped with the PCCS to the large-break loss-of-coolant accident (LBLOCA). The heat removal performances of the PCCS and the corresponding containment pressure were compared to those calculated via the original condensation model. Various thermal-hydraulic parameters associated with the natural circulation operation through the heat transport circuit were also investigated in this numerical study.

2. New empirical correlation

2.1. JNU condensation tests

For an accurate prediction of heat removal performance of the PCCS, one requires a heat transfer model which is capable of taking into account thoroughly the effect of thermal, flow conditions as well as tube dimensions on the heat transfer coefficient of the air-steam condensation. In previous studies of the authors, a comprehensive experimental database was collected through the JNU condensation test program performed at the JERICHO facility [13,14]. The schematic diagram of the JERICHO facility is shown in Fig. 3. The condensation heat transfer coefficients were measured on the exterior surface of a vertical tube of 1.0 m in effective length mounted in the test vessel, which is 1950 mm high and 609 mm in diameter. A detailed description of the experimental apparatus and the measurement, and data reduction is found in Ref. [13].

For the 40-mm-O.D. condenser tube, the heat transfer coefficients were obtained at pressure ranging from 2 to 5 bar, the air mass fraction from 0.10 to 0.88, and the wall subcooling degree between 19 and 69 K. In the research, it was revealed that the length of the condenser tube and the corresponding aspect ratio of an enclosure confining the vapor-gas mixture were very influential, as they determined characteristics of natural convection flow of the gaseous mixture, and the flow velocity around the condensing surface. Hence, Lee et al. claimed that the Grashof number should

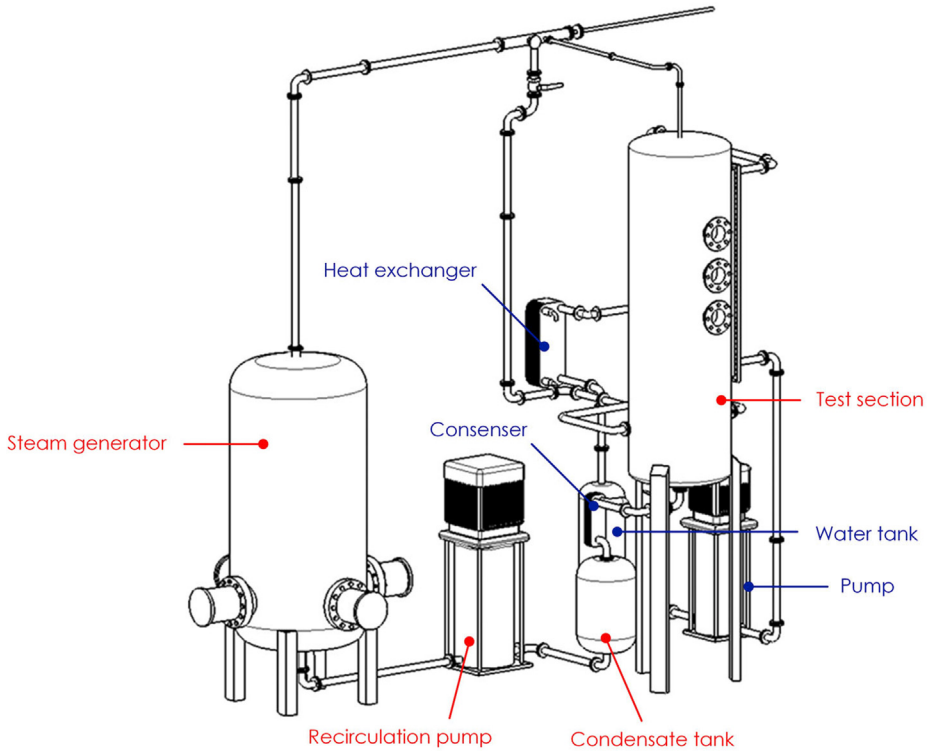

Fig. 3. A system configuration of the JERICHO facility for condensation tests. Red letters indicate components in the flow path of steam and condensate, and blue ones represent those in the cooling circuit (the secondary side) [21]. (For interpretation of the references to colour in this figure legend, the reader is referred to the Web version of this article.)

be regarded as a major factor expressing the Nusselt number of steam condensation over a vertical slender cylinder under natural convection conditions. Based on the experimental data, a new empirical correlation was proposed in a non-dimensional form where the Nusselt number was correlated in terms of the Grashof number, Jakob number, and the air mass fraction. The heat transfer coefficient calculated from the Lee correlation tended to deviate from measured data on a tube with the diameter far lower than 40 mm [15].

Recently, Kim et al. carried out subsequent condensation tests in JERICHO to elucidate the effect of the tube diameter on the air-steam condensation [14]. A new condenser tube of 21.5 mm in outer diameter was mounted in the test vessel of the JERICHO facility, and the mean heat transfer coefficients were measured to compare with those obtained on the 40-mm-O.D. tube in the previous tests.

Through two series of tests, an interesting distinction was observed visually between behaviors of the falling condensate over slender cylinders with different surface curvatures. Fig. 4 show the captured images of the condensate taken on 40-mm-O.D. and 21.5-mm-O.D. tubes during a test at 4 bar with atmospheric air present, while the surface temperature was kept almost the same [16]. In this condition, the condensing surface of the 40-mm-O.D. tube was not totally covered with the liquid condensate. A number of liquid drops grew and coalesced with neighboring ones, then eventually flowed downwards in the form of rivulets. That is, when the surface curvature was low, the condensate mass flux was not enough to cover the entire cold surface. In Fig. 4(b), however, it was observed the condensing surface was fully wetted by continuous film over the 21.5-mm-O.D. tube. The liquid film even exhibited the wavy interface in contact with the vapor-gas mixture. This implied that the condensate mass flux was larger on the 21.5-mm-O.D. tube than on the 40-mm-O.D. one, and the heat transfer coefficient relied apparently on the surface curvature when steam condensation occurred in the presence of a noncondensable gas.

Accordingly, a consistent augmentation of heat transfer coefficient was observed in the tube with a smaller diameter, i.e. higher curvature. Kim et al. reported that the heat transfer coefficient increased by 62% on average over the air mass fraction ranging from 0.1 to 0.8 when the tube diameter was reduced from 40 mm to 21.5 mm [14]. This indicates that, though the most governing factor that affects the condensation heat transfer is the concentration of noncondensable gas in the mixture, one cannot ensure an accurate estimate of the condensation heat transfer coefficient without taking into account the curvature effect. Kim et al. also claimed that the approximate correlation proposed by Popiel did not properly account for enhancement of the rate of condensation heat transfer. Hence, a new correction factor for the curvature effect was developed as a logarithmic function of the tube diameter in the form of multiplier for the Lee correlation.

2.2. Heat transfer correlation

The Lee correlation was proved to give accurate predictions for the condenser tube with moderate diameters around 40 mm as it could forecast the condensation heat transfer for a wider range of the Rayleigh number than other correlations could [15]. By introducing the correction factor for the curvature effect, one can predict the heat transfer coefficient of the air-steam condensation for any cylindrical tube with outer diameter between 21.5 and 40 mm; this range is compliant to practically adoptable tube dimensions for heat exchangers of a containment scale safety system.

Derived from JERICHO test data, the final form of the empirical correlation for the condensation heat transfer coefficient on a vertical slender cylinder under natural convection condition is represented as (Let's call it the JNU correlation hereafter.):

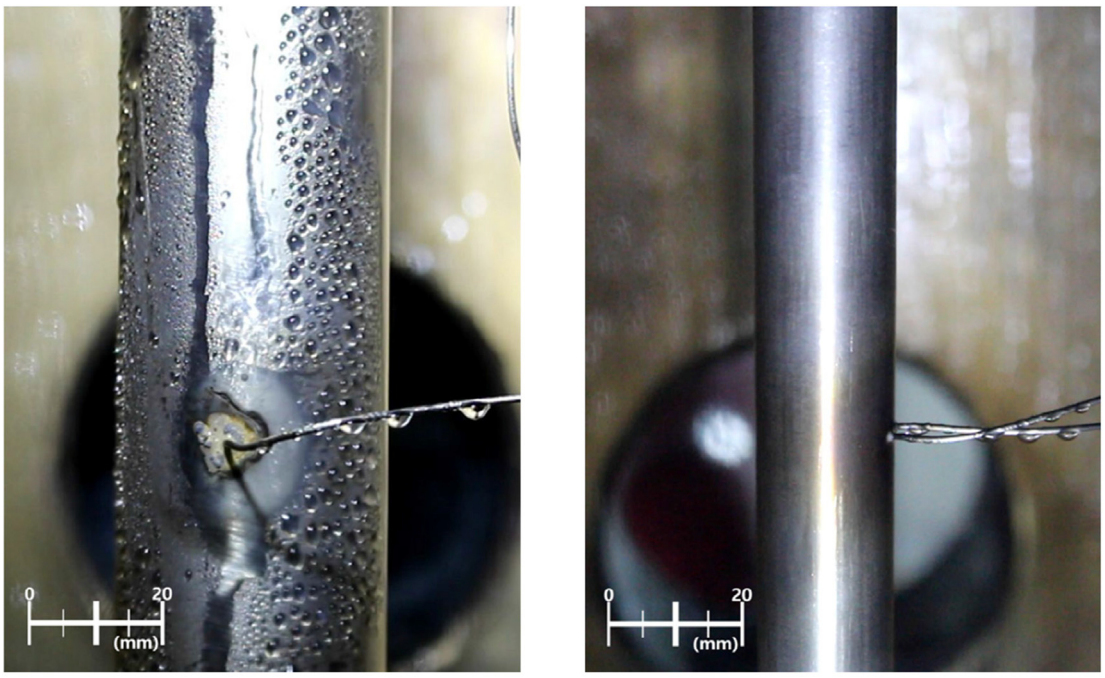

(a) 40-mm-O.D. tube (b) 21.5-mm-O.D. tube

Fig. 4. Visualized behavior of the liquid condensate formed on the exterior surface of cylindrical tubes with different surface curvature (pressure: 4 bar, air mass fraction: 0.35, Wall subcooling degree ~ 40 K). The recorded video files are available as supplementary data in Appendix A.

$$\overline{Nu}_D = \overline{Nu}_0 \cdot \eta, \tag{1}$$

where

$$\overline{Nu}_0 = 890\ Gr_L^{0.125} W_s^{*0.966} Ja^{-0.327}, \tag{2}$$

and the multiplier for the tube diameter η is given as:

$$\eta = D^*(1 - 1.21 \ln D^*). \tag{3}$$

W_s^* in Eq. (2) was empirically defined as:

$$W_s^* = 1 - W_a^{0.01}, \tag{4}$$

and D^* in Eq. (3) is the normalized diameter expressed as $D^* = D/D_0$, where D_0 represents the reference diameter (0.04 m). That is, the proposed correlation was developed to calculate the mean Nusselt number for the base tube, and correct the deviation caused by the curvature effect on condensation heat transfer with the multiplier expressed as Eq. (3). The proposed correlation is valid over the ranges:

$$0.54 \le D^* \le 1.0$$

$$1.36 \cdot 10^{10} \le Gr_L \le 5.05 \cdot 10^{12}$$

$$1.16 \cdot 10^{-3} \le W_s^* \le 5.05 \cdot 10^{-2}$$

$$0.009 \le Ja \le 0.035$$

The new empirical correlation, Eq. (1), was implemented into the MARS-KS code in this study so that more realistic prediction can be acquired on the heat transfer performance of heat exchangers in the PCCS. Before applying the modified code to the containment analysis, we validated the implemented condensation model by using the experimental data from MIT tests and JERICHO tests.

3. Implmentation of new correlation to MARS-KS

3.1. Default model

For condensation in the presence of a noncondensable gas, the MARS-KS code applies the Colburn-Hougen diffusion method. This method assumes co-existing boundary layers of the liquid condensate and the vapor-gas mixture on the condensing surface. It neglects sensible heat transfer through the diffusion layer to the liquid-vapor interface, and obtains the mass transfer coefficient by applying the analogy between heat and mass transfer. The formulation is based on the energy balance between two boundary layers; the rate of heat transfer by condensation of steam that diffuses from the bulk to the liquid-vapor interface is equal to that across the liquid condensate [17].

The heat flux across the liquid condensate is calculated by:

$$q_l'' = h_c(T_{vi} - T_w), \tag{5}$$

where h_c is the heat transfer coefficient in the liquid film, and T_{vi} is the temperature of the liquid-vapor interface, which is equal to the saturation temperature corresponding to the vapor partial pressure at the interface. h_c is determined as the maximum of the heat transfer coefficient by the Nusselt model for laminar flow [18] and that by Shah's correlation for turbulent flow [19].

The heat flux due to condensation of vapor mass flux in the diffusion layer is:

$$q''_v = h_m h_{fgb} \frac{\rho_{vb}}{\chi_{vb}} \ln\left(\frac{1 - P_{vi}/P}{1 - P_{vb}/P}\right), \quad (6)$$

where h_m denotes the mass transfer coefficient, ρ_{vb} and x_{vb} are the saturation vapor density and the vapor mole fraction in the bulk, respectively. Applying the heat and mass transfer analogy, the MARS-KS code calculates the mass transfer coefficient as the maximum value predicted from laminar or turbulent forced convection correlations and a natural convection correlation. These correlations determine Sherwood number expressed as:

$$Sh = \frac{h_m D}{D_{vn}}, \quad (7)$$

where D and D_{vn} are the hydraulic diameter and the mass diffusivity, respectively. The mass transfer correlations for each flow regime are summarized in Table 1. Since the temperature difference across each boundary layer as well as the heat transfer coefficient in the liquid condensate rely on the liquid-vapor interface temperature, the numerical model in the MARS-KS finds T_{vi} that balances the heat flux across the diffusion layer and that from the liquid film to the wall, i.e. $q''_l = q''_v$, by the iteration scheme.

3.2. MARS-KS modeling

The JNU correlation, Eq. (1), developed based on JERICHO test programs was implemented into the subroutine 'noncnd' of the MARS-KS code, which is incorporated to calculate the wall-to-fluid heat transfer by steam condensation in the presence of a noncondensable gas. The correlation was coded in a way that, if the heat transfer hydraulic diameter on the outer wall of the cylindrical heat structure is less or equal to the upper bound for the JNU correlation ($D^* \leq 1.0$), the heat structure was regarded as the cylindrical tube in the heat exchanger and the heat flux was estimated based on Eq. (1) without an iteration process. Otherwise, the heat flux was calculated by the default model as is; then, for example, the heat transfer rate on the passive heat sink (structural walls etc.) in the containment would be evaluated by the default model.

The valid range of the Grashof number for the JNU correlation corresponds to the tube length between 1.0 m and 3.5 m. When the simulated condenser tube is longer than 3.5 m, the length of the condenser tube used in MIT tests, the implemented model was set to take this upper limit as the characteristic length for the Grashof number. This approach is based on the assumption that, as the cylindrical vessel of MIT tests had very high aspect ratio on account of a lengthy condenser tube, natural convective flow of the vapor-gas mixture was vigorous enough to simulate flow conditions in the containment caused by even longer condenser tubes in the PCCS.

On a longer vertical tube, the liquid condensate will be accumulated and its thickness will grow as the condensing length increases. In the presence of a noncondensable gas, however, the heat flux on the condensing surface is dominated by the thermal resistance of the vapor-gas boundary layer, not by that across liquid film; this is the more so when the mass fraction of a noncondensable gas is high alike the transient in the containment. Thus, a drastic reduction of the local heat transfer coefficient by the accumulated condensate is not expected. On the other hand, it has been reported from a numerical study that, since the density of the gas mixture is higher near the liquid-vapor interface than in the bulk, the gas mixture is accelerated along the wall and the gas velocity increases with the condensing length [20]. This enhances the turbulent diffusivity, and thus the transport of gas species.

Users should note that, when modeling the condenser tube in the PCCS, they have to use 12-word format or 13-word format cards, not 9-word format cards, for additional right boundary conditions to input the natural circulation length, which is used as the characteristic length for the Grashof number in Eq. (2). In addition, the outer diameter of the condenser tube should be given in the card for the heat transfer hydraulic diameter of the heat structure, whatever model is applied, since it determines the mass transfer coefficient from the Sherwood number in the default model or the correction factor in the JNU correlation. If it is entered as 0.0, then the code will regard the hydraulic diameter of the associated hydrodynamic volume as the outer diameter of the condenser tube [21].

Fig. 5 presents the nodalization to model the test section of the JERICHO facility by the MARS-KS code. The test vessel was modeled with six single volumes connected by single junctions. The internal volume of the test vessel was divided radially into two columns of nodes having the same cross-sectional area in order to simulate the flow path of naturally circulating flows of the air-steam mixture. It was confirmed from the sensitivity test of nodalization that, though the circulation flow rate of the air-steam mixture through connecting junctions somewhat varied depending on the area ratio between C200 and C350, the mean heat transfer coefficient was little affected by this area ratio [22]. This is attributed to the fact that both the default model and the implemented correlation are not expressed directly as a function of the gas mixture velocity in the vicinity of the condensing surface.

Note that the hydrodynamic volume with which the heat structure for the condenser tube was associated (C350) was modeled by the single volume, not by the pipe with multiple nodes. This is because a uniform distribution of the air-steam mixture was sustained during JERICHO tests, and we focused on simulating the same thermal conditions as the experiment. The preliminary study revealed that employing multiple nodes for C350 brought little difference in the predicted mean heat transfer coefficient [22].

Regarding the boundary conditions, the steam was supplied from the time dependent volume C100 to C150 at a saturation pressure corresponding to the measured gas temperature in the bulk. The steam mass flow into the test section was adjusted by the time dependent junction C125 so that the injection rate is proportional to the deviation of the calculated vessel pressure represented by C350 from a preset pressure. In order to implement the same wall temperature to the condensing surface (the right boundary in the heat structure) as the test condition, the measured average wall temperature was given as the left surface temperature

Table 1
Correlations for the mass transfer coefficient in the diffusion layer.

Flow regime	Authors	Correlation for h_m
Laminar	Rohsenow and Choi	$Sh = 4$
Turbulent	Gilliand	$Sh = 0.023 Re^{0.83} Sc^{0.44}$
Natural	Churchill and Chu	$Sh = \left\{0.825 + \frac{0.387 Ra_L^{1/6}}{\left[1 + (0.492/Sc)^{9/16}\right]^{8/27}}\right\}^2$

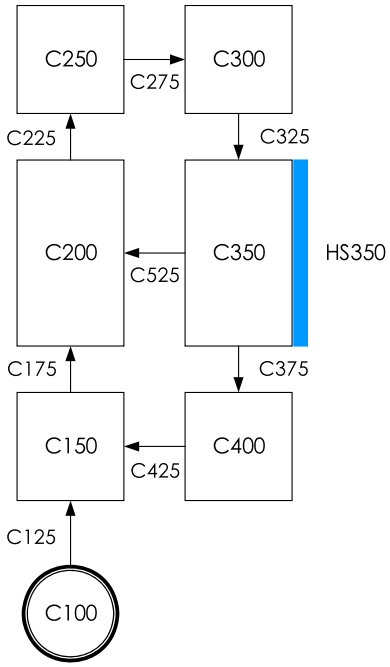

Fig. 5. MARS-KS nodalization for JNU condensation experiments.

and an arbitrary, very high thermal conductivity and volumetric heat capacity were imposed on the property data to make the temperature gradient across the wall negligible. Then the condensation heat transfer coefficient was calculated by:

$$\overline{h} = \frac{q''}{T_b - T_w}, \tag{8}$$

where the heat flux in the numerator is the one calculated by the Colburn-Hougen model or the JNU correlation, and T_b denotes the gas temperature in the bulk region of C350.

The liquid condensate from C350 is collected to C400. Even for the test run where the condensation heat transfer rate was the highest, i.e. the test at 5 bar with the air mass fraction of 0.1, the collected volume of the condensate for the entire calculation time was less than 2% of the volume of C400. Thus, the effect of the collected liquid condensate could be assumed negligible. The heat loss from the test vessel was not taken into account in the MARS-KS model because the heat transfer rate on the condenser tube is independent of the heat loss as long as the bulk conditions are fixed.

3.3. Assessment result

Fig. 6 present the calculation results for JNU tests, with the 40-mm-O.D. tube and the 21.5-mm.O.D. tube, and MIT tests by using the original and modified versions of the MARS-KS code. With the default model, the calculated heat transfer coefficients for the base tube of the JERICHO facility were comparable to measured experimental data. When the tube diameter became small or a longer condenser tube was deployed, however, the original MARS-KS code underestimated substantially the condensation heat transfer coefficient as shown in Fig. 6(b) and (c). The default model for steam condensation was unable to forecast the variation in the heat transfer coefficient by the surface curvature, nor the enhancement of heat transfer by a violent flow field arising from a lengthy condensing surface; its prediction only relied on thermal conditions in the bulk and on the wall, and the composition of the gaseous mixture. As aforementioned, the conservative prediction on the rate of heat removal from a passive heat exchange device is unsatisfactory regarding it will drive the design decision to demand a larger heat transfer area than the best-estimated value.

As presented in Fig. 6, the prediction accuracy of the MARS-KS code was much improved by implementing the JNU correlation, for it considered the geometric effect of the cylindrical tube as well as the relationship with the naturally induced flow behavior characterized by the Grashof number. The average deviation was reduced from 53% to 8.1% for JNU tests with the 21.5-mm-O.D. tube, 53%–6.0% for MIT tests through the modification of the steam condensation model. This implies that the modified MAR-KS code is capable of performing more realistic analysis of the containment transient with the PCCS on operation than the original one. We applied the modified MARS-KS code for evaluating the containment response to the loss-of-coolant accident accompanied by enormous stream release and the heat removal performance of the prototypical PCCS, as present in the next section.

4. Containment transient simulation

4.1. Problem statement

As illustrated in Fig. 1, the PCCS heat exchangers are connected to two large water pools, called passive containment cooling tanks (PCCTs), located on the top of the auxiliary building. Since iPOWER employs four trains of the PCCS, each PCCT is shared by two trains of the PCCS. While the PCCS is on operation, the cooling water is fed through the supply line to the inlet distribution header from which the cooling water is distributed to bundle headers of the heat exchanger assemblies, and condenser tubes, subsequently. Then the cooling water heated inside condenser tubes is collected at the outlet bundle headers and exits from the distribution header to return to the PCCT. The return pipeline is connected to the side wall of the PCCT just below the initial water surface. The PCCT is assumed open to the atmosphere so that no pressurization would occur in the PCCT or the natural circulation circuit of the PCCS.

Simulation conditions are determined based on the provisional design dimensions of the PCCS and the containment information available for an existing nuclear power plant, as summarized in Table 2 [23]. The reference plant is set to Shin-Hanul Units 3 and 4 with APR1400 reactors. The accident progression by the LBLOCA accompanied by the maximum safety injection rate is assumed. A train of the PCCS consists of eight heat exchanger assemblies, each housing 252 (6 × 42 arrays) condenser tubes of 31.75 mm in outer diameter and 6 m in length [24]. The PCCT and the natural circulation circuit are initially filled with quiescent water in temperature of 49 °C.

Passive safety systems are generally required to perform their safety functions, without relying upon operators action or offsite support, for at least 72 h after an initiating event [25]. Therefore, this numerical study evaluates the containment transient managed by the PCCS for 200,000 s.

4.2. Modeling of the containment and PCCS

The MARS-KS nodalization of the containment and the PCCS is presented in Fig. 7. The input deck to investigate the containment pressure response was developed in the study of Lim et al. [23]. The containment dome is modeled as a single volume (C500), and the cylindrical part is modeled by five pipe components and two single volumes; the heat exchangers of the PCCS are located at single volumes C300 and C400. The PCCT is modeled as a pipe component containing 25 volumes. The lower 18 vol are initially filled with water, and the top of the PCCT is connected to a time-dependent

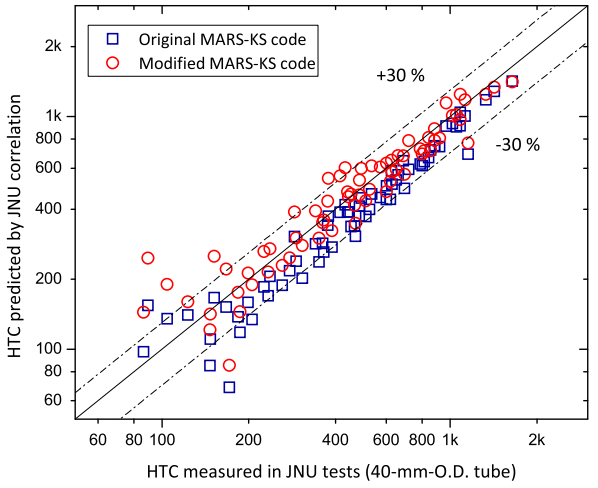

(a) JNU tests with the 40-mm-O.D. tube

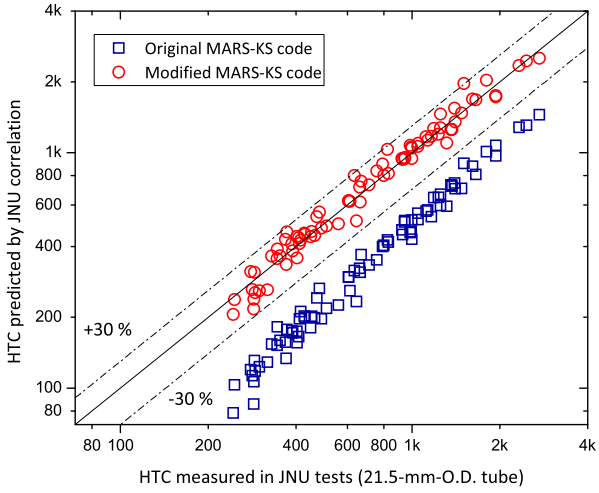

(b) JNU tests with the 21.5-mm-O.D. tube

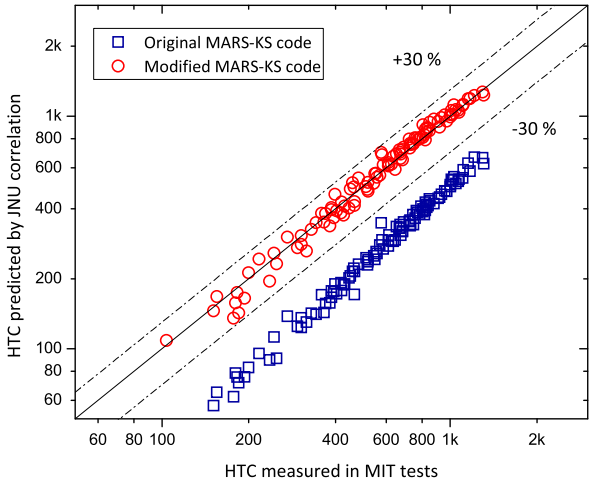

(c) MIT tests with the 38-mm-O.D. tube

Fig. 6. Improved prediction results by the modified MARS-KS code with the new correlation of the condensation heat transfer coefficient for JNU tests and MIT tests.

volume component to specify the pressure boundary maintained at the atmospheric pressure.

Condenser tubes in the heat exchanger assembly are modeled as a pipe component consisting of 12 vertical volumes. That is, each train of the PCCS is described by eight lumped pipe components, with the total hydrodynamic volume preserved, as shown in Fig. 7. Branch components are used to simulate the distribution headers and the bundle headers; the inlet and outlet bundle headers of each train were modeled by eight sequentially numbered components (for instance, C651 – C658 for inlet bundle headers of the first train). The supply line, the riser section, and the horizontal return line are modeled as pipe components containing 52, 17, and 30 vol, respectively. Heat structures are provided at the hydrodynamic volumes of the heat exchanger to simulate the heat transfer by steam condensation and connected to containment volumes C300 and C400. Passive heat sinks of the containment such as the concrete wall, liner plate, embedment concrete, and miscellaneous steels are also modeled as heat structures, on the basis of the design information of Shin-Hanul Units 3 and 4.

For convenience, instead of modeling all the reactor coolant system, we implemented the mass and energy release data due to the postulated LBLOCA as the boundary condition (See Fig. 8 for the energy release data.). The time-varying saturation pressure of the reactor coolant system is defined using a time-dependent volume component, and the discharge rates of steam and water are specified by two separate time-dependent junction components connected to the third volume of C100.

4.3. Calculation results and discussions

Fig. 8 presents the energy release rate due to coolant discharge, given as the boundary condition, and the heat removal rate by the passive heat sink (PHS) and the PCCS. The evolution of the containment pressure, shown in Fig. 9, depends on the relative magnitude of the heat addition to the atmosphere of the containment and the heat rejection by steam condensation. During the initial blowdown phase, very large amount of coolant discharges from the primary coolant system, resulting in a rapid accumulation of energies inside the containment; within 10 s, the energy release rate is at least an order of magnitude larger than the total heat removal rate. This causes a drastic rise of the containment pressure up to 390 kPa in just 28 s. Then, the containment pressure starts to decrease from the peak as the coolant discharge rate is reduced and the heat removal by the PHS and the PCCS increases.

Note that, in the early phase of the transient, most of heat removal from the containment is achieved by the passive heat sink while the contribution of the PCCS remains minor. In spite of high wall subcooling degree of the condenser tube, a high air fraction in this early phase (See Fig. 12) retards substantially the steam condensation rate on the PCCS heat exchanger. However, as the air fraction in the gaseous mixture is lowered by continuous steam release and the natural circulation of the cooling water is initiated inside condenser tubes, the heat removal rate of the PCCS grows fast and peaks at 28 s. At 1450 s after the initiating event, the heat removal rate of the PCCS exceeds that of the passive heat sink, and the cooling of the containment is dominated by the PCCS since then. The containment pressure continues to reduce to 212 kPa at 12,000 s. However, on account of the sustained rise of the cooling water temperature in the PCCT (Fig. 10) and the corresponding decrease in the wall subcooling degree on condenser tubes (Fig. 11), the containment building is pressurized again.

The calculation results of the cooling water temperature and the mean wall subcooling degree of condenser tubes are presented in Figs. 10 and 11. As the heat transport by steam condensation begins, the outlet temperature of cooling water in the PCCS heat

Table 2
Simulation conditions of the containment pressure transient.

Parameters	Values
Containment data	
Reference plant	Shin-Hanul Units 3 and 4 (APR1400)
Containment free volume (m^3)	8.9×10^4
Accident condition	LBLOCA with the maximum safety injection
PCCS data	
Number of the train	4
Number of the HX assembly per train	8
Number of the condenser tube per assembly	252
Tube diameter (mm)/length (m)	31.75/6.0
PCCT data	
Number of the tank	2
Initial water level (m)	9.0
Water volume (m^3)	2780

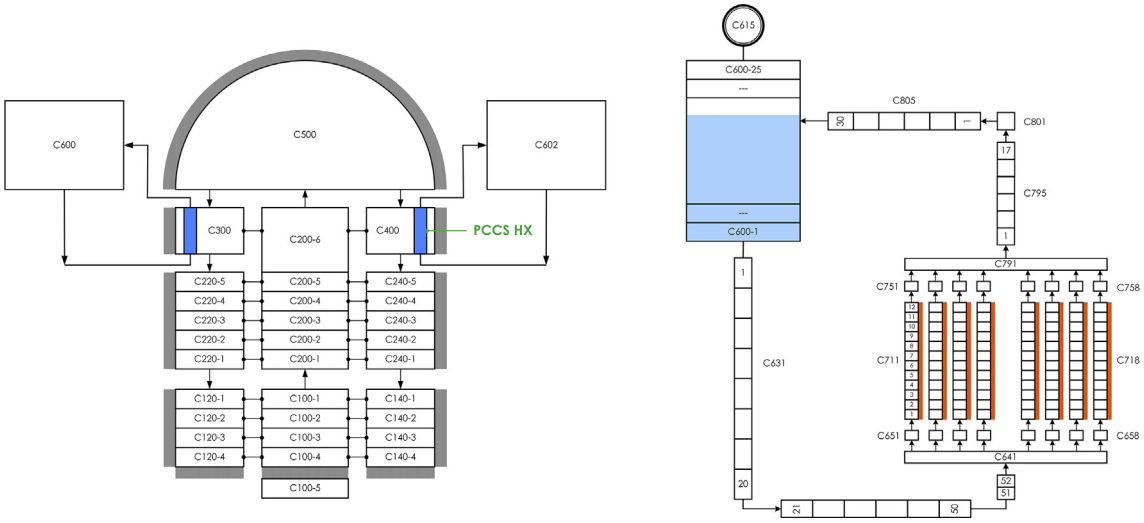

Fig. 7. MARS-KS nodalization of the containment building and the PCCS (Component numbers marked in the right figure are those specified for the first train of the PCCS.).

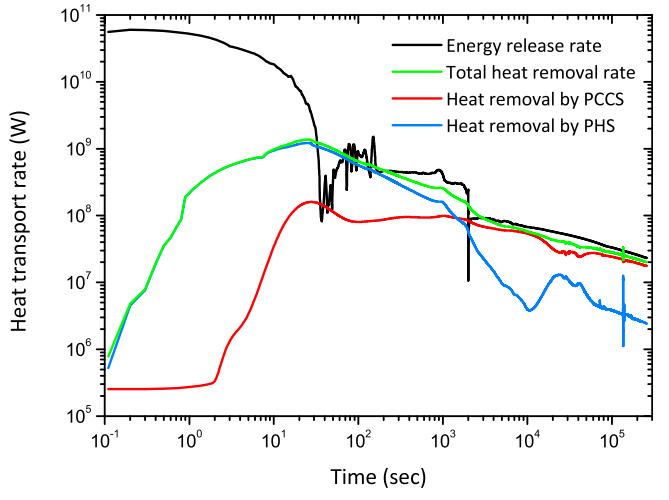

Fig. 8. Energy release rate into the containment and calculated heat removal rate by the PCCS and the passive heat sink in the transient initiated by the LBLOCA.

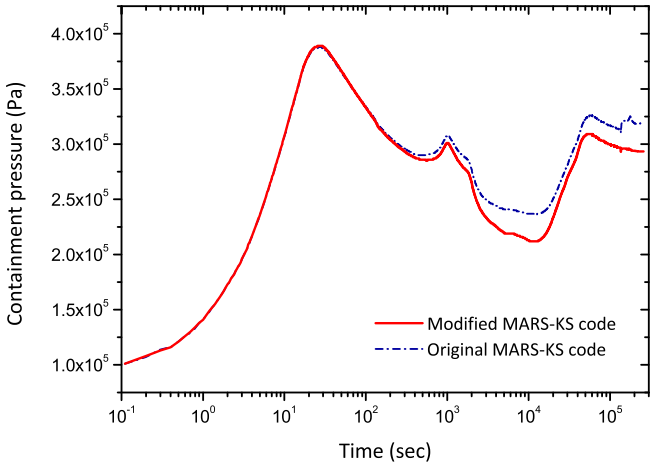

Fig. 9. The pressure response of the containment predicted by the modified MARS-KS code and the original one.

exchangers rises quickly, whereas the inlet temperature varies little owing to a large water volume in the PCCT until 10,000 s. Thereafter, as soon as the heated cooling water from the PCCS is supplied, both of the inlet and the outlet temperature of the PCCS heat exchangers continue to increase. However, the cooling water does not reach the saturation condition until the end time of the problem due to the hydrostatic head in the return line and the PCCT. The

heat transfer mode inside condenser tubes remains the single-phase liquid convection regime throughout the whole period of the transient, a significant void fraction does not appear even at the exit of the heat exchangers until 200,000 s. On the other hand, the lowered hydrostatic pressure at elevated volumes in the riser section of the return line allows cooling water to reach the saturation condition from 28,000 s, resulting in the onset of flashing.

With regard to the wall subcooling degree, it is one of crucial factors governing the rate of heat transfer by the air-steam condensation. It is revealed that, except for very early phase of the transient, the average wall subcooling degree on condenser tubes remains lower than 20 K. After 10,000 s, as the cooling water in the PCCT heats up, followed by the rise of the inlet temperature of cooling water into the PCCS heat exchangers, the mean wall subcooling degree further decreases below 10 K. The previous experimental work in the JERICHO facility [13] and that from Pusan National University [26] have reported that, even though the condensation heat transfer coefficient itself increased with the rise of the wall temperature, the rate of heat transfer was reduced substantially in such a low-wall subcooling region. That is, the heat removal performance of the PCCS heat exchangers is kept much lower than their optimum capacities for most period of the transient, and this is why a limited suppression of the rise of the containment pressure is to be achieved for a long-term period, as shown in Fig. 9, by natural circulation cooling.

Fig. 12 show the variation of the air quality in the gaseous mixture inside the containment building. Since this study assumes no additional generation of noncondensable gases during the accident progression, the relative fraction of air varies depending on the containment pressure. The air quality inside the containment is not less than 40%, which is the value reached when the containment pressure peaks at 28 s. As shown in Fig. 13, the water level in the PCCT rises very slowly with an increase of the cooling water temperature in the natural circulation circuit until the flashing in the return line generates vapor phases and thus causes continuous loss of the water inventory inside the PCCT.

Fig. 14 presents the variation of the natural circulation flow rate of the cooling water per train. It is mainly influenced by the rate of heat transport from the outer side of the PCCS heat exchangers and the voids generation. A stable natural circulation flow in the single-phase liquid state is established until the vapor generation begins and the transition to the two-phase natural circulation mode occurs at around 28,000 s. The flashing in the riser section augments the difference of the hydrostatic head between the downward channel (PCCT + supply line) and the upward channel (heat exchanger + return line), which leads to an increase in the flow

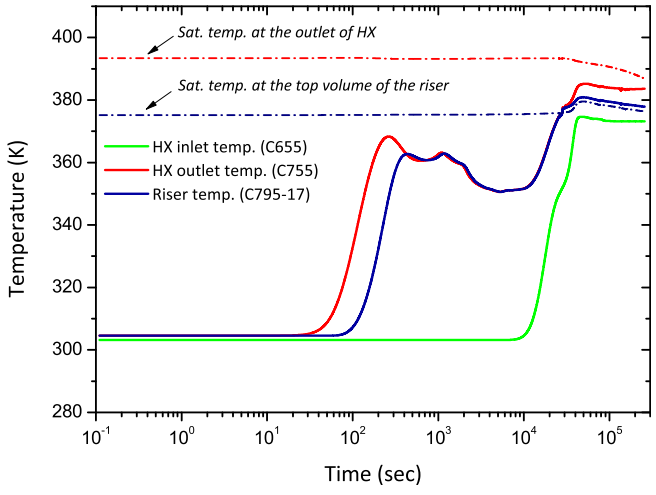

Fig. 10. Changes of the temperature of cooling water in the PCCS heat exchangers and the return line.

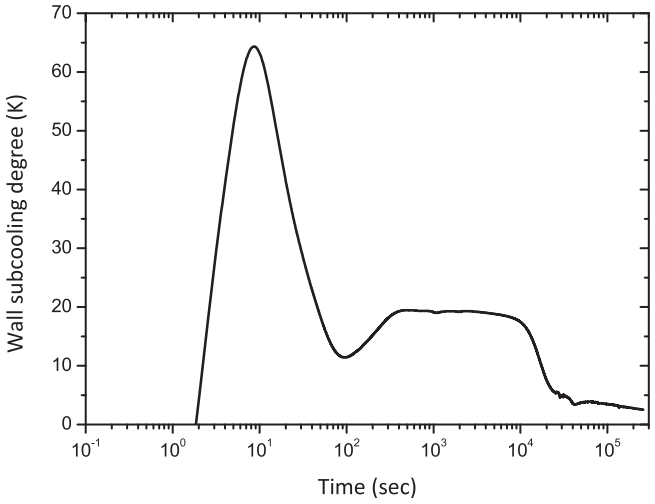

Fig. 11. Calculated wall subcooling degree on the exterior surface of condenser tubes.

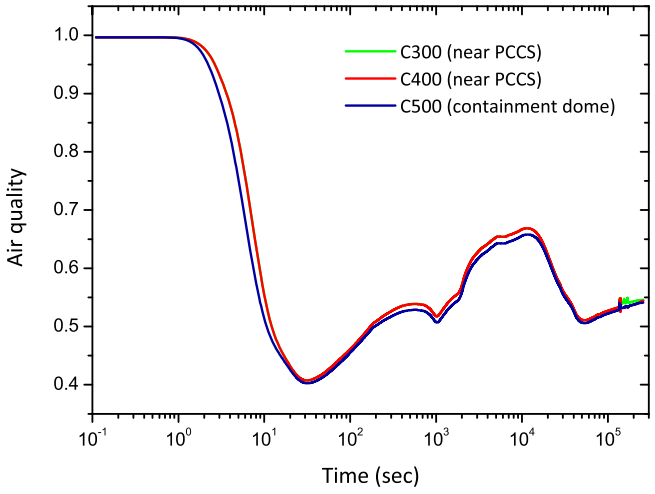

Fig. 12. The air quality inside the containment building.

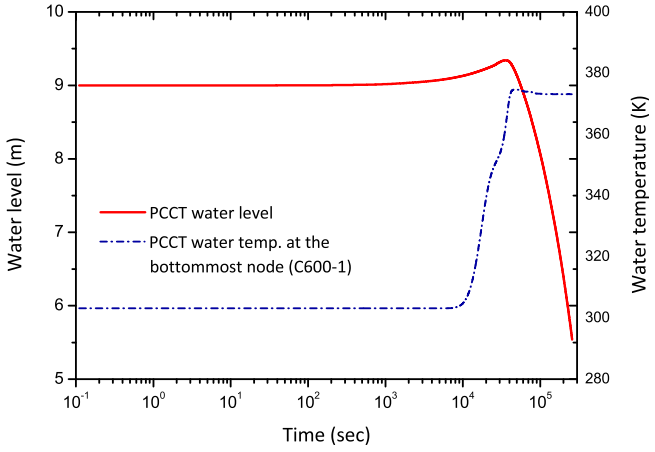

Fig. 13. Changes in the collapsed water level and the water temperature in the PCCT.

rate. The reduction in the condensation heat transfer by the rise of air quality and the loss of wall subcooling degree could be compensated by the enhancement of in-tube heat transfer arising from the increased natural circulation flow rate. Therefore, the containment pressure decreases during the late phase of the transient, even though its rate of change is very slow.

In Fig. 9, the change of the containment pressure predicted by the original MARS-KS code is also plotted to indicate the effect of the steam condensation model selected for the PCCS. Fig. 9 implies that, if the default Colburn-Hougen model is applied, the heat removal of the PCCS tends to be underestimated. The minimum containment pressure at 12,000 s calculated by the original MARS-KS code deviates from that predicted from the modified code by 25 kPa. That is, the default condensation model is likely to provide the conservative prediction on the pressure response of the containment, with less margin to fulfill the safety requirement for the PCCS. For the default model, the Sherwood number in natural convection regime is calculated based on the Rayleigh number as shown in Table 1, but the mass transfer coefficient itself rarely varies with the natural circulation length. In this study, we tried to be more realistic by taking into account the effect of the flow field around the PCCS on the basis of a new correlation as a function of the Grashof number.

The simulation results in Fig. 9 also indicate that the long-term cooling capability of the PCCS may not be sustained as much as to keep the containment pressure decreasing in time. The numerical analysis forecasts that the containment will suffer from re-pressurization in 4 h after the initiating event due to loss of the wall subcooling of the PCCS heat exchangers. After reaching its peak value at around 30 s, the heat removal performance of the PCCS continues to degrade throughout the transient as shown in Fig. 8. By the nature of the passive safety system, the PCCS is unable to exhaust accumulated energy from the cooling water by itself. It is turned out from this study that it is not a matter of thermal sizing of heat exchangers in the PCCS; regaining a sufficient heat removal rate is associated with restoring high wall subcooling degree of condensing surfaces, namely, by lowering the temperature of the cooling water in the natural circulation circuit. For instance, if operators supply cold water to the PCCT after 72 h, from which we can assume a follow-up accident management becomes possible, then the wall subcooling degree of condenser tubes will rise and, in turn, the containment pressure will be stabilized. Otherwise, in order to delay the temperature rise of cooling water during the transient, one may come up with implementing devices for further cooling the PCCT such as heat pipes.

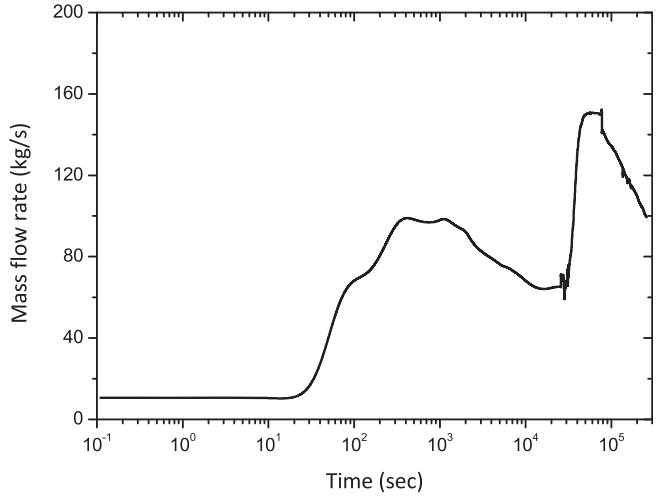

Fig. 14. The mass flow rate per train by natural circulation between condenser tubes and the PCCT.

5. Conclusions

A new empirical correlation of the steam condensation model proposed by Jeju National University was implemented into the MARS-KS code to correct the conservative prediction of the heat transfer coefficient on a longer cylindrical tube, which induces a higher free stream velocity of the circulating gas mixture around the condensing surface. The modified MARS-KS code was assessed against experimental data from MIT tests and JNU tests, and the improved calculation accuracy was achieved over a wide range of the Grashof number for the air-steam condensation under natural convection conditions.

The modified MARS-KS code was applied to simulation of the transient response of the containment equipped with the PCCS to the large-break loss-of-coolant accident. It was revealed that, depending on the choice of the steam condensation model for the PCCS, the transient containment pressure could be deviated by as much as 25 kPa under LBLOCA conditions. The default steam condensation model of the MARS-KS code was likely to underestimate the heat removal performance of the PCCS. If we desire to design a PCCS that fulfills the safety requirement defined in terms of the containment pressure, it would seem as if the safety margin is very limited than its actual level as long as we rely on the default condensation model for its performance evaluation. On the contrary, we can realize savings in the cost and the required space for installation of the PCCS in the containment when design decisions are made based on the new correlation, which is more realistic.

Whatever condensation model we applied, the analysis results indicated that inevitable loss of the wall subcooling of the PCCS heat exchangers in time was turned out to restrict the long-term cooling capability of the PCCS as well as the suppression of the containment pressure. This necessitates follow-up supports to supply cooling water into the heated PCCT or implementation of cooling devices for the PCCT to terminate the pressure transient in the containment.

As a future work, we intend to investigate experimentally the effect of the flow velocity on the condensation heat transfer coefficient on a cylindrical tube through the forced convective condensation test using the JERICHO facility. Unlike the aforementioned JNU tests performed on natural circulation, the flow velocity of the gaseous mixture can be directly controlled by employing a separate test section for forced convection [27]. This will help to evaluate the adequacy of the modified MARS-KS code as an analysis tool to best-estimate the cooling performance of the PCCS for a wide range of the free stream velocity.

Declaration of competing interest

The authors declare that they have no known competing financial interests or personal relationships that could have appeared to influence the work reported in this paper.

Acknowledgements

This work was supported by the research grant of Jeju National University in 2019.

Appendix A. Supplementary data

Supplementary data to this article can be found online at https://doi.org/10.1016/j.net.2021.04.024.

Nomenclature

D	Diameter (m)
D_0	Normalizing diameter (m)
D_{vn}	Mass diffusivity ($m^2\ s^{-1}$)
D^*	Normalized diameter
Gr	Grashof number
h_c	Heat transfer coefficient in the liquid film ($W\ m^{-2}\ K^{-1}$)
h_{fg}	Latent heat ($J\ kg^{-1}$)
h_m	Mass transfer coefficient ($kg\ m^{-2}s^{-1}$)
HX	Heat exchanger
$\overline{h}$	Average heat transfer coefficient over length ($W\ m^{-2}\ K^{-1}$)
Ja	Jakob number
L	Length (m)
$\overline{Nu}$	Average Nusselt number over length ($W\ m^{-2}\ K^{-1}$)
$\overline{Nu}_0$	Average Nusselt number for the referenced diameter, 40 mm ($W\ m^{-2}\ K^{-1}$)
P	Pressure (Pa)
q''	Heat flux ($W\ m^{-2}$)
Ra	Rayleigh number
Sc	Schmidt number
Sh	Sherwood number
T	Temperature (K)
W	Mass fraction
x	Mole fraction

Greek letters

η	Correction factor for the curvature effect
ρ	Density ($kg\ m^{-3}$)

Subscript

a	Air
b	Bulk conditions
i	Liquid-vapor interface
l	Liquid condensate
s	Steam
w	Wall
v	Vapor

References

[1] T.L. Schulz, Westinghouse AP1000 advanced passive plant, Nucl. Eng. Des. 236 (2006) 1547–1557.

[2] A.M. Shabestary, F. Viereckl, Y. Zhang, R. Manthey, D. Lucas, C. Schuster, S. Leyer, A. Hurtado, U. Hampel, Modelling of passive heat removal systems: a review with reference to the Framatome KERENA BWR reactor: Part I, Energies 13 (2020) 35–68.

[3] S.W. Lee, S. Heo, H.U. Ha, H.G. Kim, The concept of the innovative power reactor, Nucl. Eng. Technol. 49 (2017) 1431–1441.

[4] Y. Kozmenkov, U. Rohde, A. Manera, Validation of the RELAP5 code for the modeling of flashing-induced instabilities under natural-circulation conditions using experimental data from the CIRCUS test facility, Nucl. Eng. Des. 243 (2012) 168–175.

[5] M.M. Stempniewicz, M.L.F. Slootman, H.T. Wiersema, Validation of system codes RELAP5 and SPECTRA for natural convection boiling in narrow channels, Nucl. Eng. Des. 307 (2016) 130–143.

[6] X. Hou, Z. Sun, W. Lei, Capability of RELAP5 code to simulate the thermal-hydraulic characteristics of open natural circulation, Ann. Nucl. Energy 109 (2017) 612–625.

[7] Y.-J. Chung, H.-C. Kim, B.-D. Chung, M.-K. Chung, S.-Q. Zee, Two phase natural circulation and the heat transfer in the passive residual heat removal system of an integral type reactor, Ann. Nucl. Energy 33 (2006) 262–270.

[8] J.-J. Jeong, K.S. Ha, B.D. Chung, W.J. Lee, Development of a multi-dimensional thermal-hydraulic system code, MARS 1.3.1, Ann. Nucl. Energy 26 (1999) 1611–1642.

[9] A.P. Colburn, O.A. Hougen, Design of cooler condensers for mixtures of vapors with noncondensing gases, Ind. Eng. Chem. 26 (1934) 1178–1182.

[10] C.-J. Choi, J.-H. Lee, H.-K. Cho, G.-C. Park, Assessment of condensation models in the presence of noncondensable gases with vertical rectangular duct and in-tube tests using MARS and TRACE, in: Korean Nuclear Society Spring Meeting, Jeju, Korea, May 18-19, 2017.

[11] H.-M. Bang, Y.-G. Lee, Analysis of steam condensation in the presence of noncondensable gases using MARS-KS code, in: Korean Nuclear Society Spring Meeting, Jeju, Korea, May 12-13, 2016.

[12] A.A. Dehbi, The Effects of Noncondensable Gases on Steam Condensation under Turbulent Natural Convection Conditions, Ph. D. dissertation, Massachusetts Institute of Technology, 1991.

[13] Y.-G. Lee, Y.-J. Jang, D.-J. Choi, An experimental study of air–steam condensation on the exterior surface of a vertical tube under natural convection conditions, Int. J. Heat Mass Tran. 104 (2017) 1034–1047.

[14] U.-K. Kim, J.-W. Yoo, Y.-J. Jang, Y.-G. Lee, Measurement of heat transfer coefficients for steam condensation on a vertical 21.5-mm-O.D. tube in the presence of air, J. Nucl. Sci. Technol. 57 (2020) 905–916.

[15] Y.-G. Lee, Y.-J. Jang, S. Kim, Analysis of air-steam condensation tests on a vertical tube of the passive containment cooling system under natural convection, Ann. Nucl. Energy 131 (2019) 460–474.

[16] U.-K. Kim, J.-W. Yoo, Y.-J. Jang, Y.-G. Lee, Development of a correction factor for curvature effect on condensation heat transfer coefficients on a cylindrical tube, in: Korean Nuclear Society Autumn Meeting, Gyeongju, Korea, October 26-27, 2017.

[17] B.D. Chung, S.W. Bae, S.W. Lee, C. Yoon, M.K. Hwang, K.D. Kim, J.J. Jeong, MARS Code Manual Volume V: Models and Correlations, Korea Atomic Energy Research Institute, 2010. KAERI/TR-3872/2009.

[18] W. Nusselt, Die oberflachenkondensation des wasserdamphes, Z Vereines Deutsch Ing 60 (1916) 541–546.

[19] M.M. Shah, A general correlation for heat transfer during film condensation inside pipes, Int. J. Heat Mass Tran. 22 (1979) 547–556.

[20] J. Lee, G.-C. Park, H.K. Cho, Improvement of CUPID code for simulating film-wise steam condensation in the presence of noncondensable gases, Nucl. Eng. Technol. 47 (2015) 567–578.

[21] B.D. Chung, K.D. Kim, S.W. Bae, J.J. Jeong, S.W. Lee, M.K. Hwang, MARS Code Manual Volume II: Input Requirements, Korea Atomic Energy Research Institute, 2010. KAERI/TR-2811/2004.

[22] Y.-J. Jang, Experimental and Numerical Investigation of Condensation Heat Transfer on the Vertical Tube under Natural Convection Condition, Ph. D. dissertation, Jeju National University, 2018.

[23] S.-G. Lim, D.-H. Kim, J.-M. Lee, S.-W. Lee, H.-G. Kim, H.-C. No, Prediction of heat removal performance for passive containment cooling system using MARS-KS code version 1.14, in: Korean Nuclear Society Spring Meeting, Jeju, Korea, May 18-19, 2017.

[24] S.G. Lim, H.C. No, S.W. Lee, H.G. Kim, J. Cheon, J.M. Lee, S.M. Ohk, Development of stability maps for flashing-induced instability in a passive containment cooling system for iPOWER, Nucl. Eng. Technol. 52 (2020) 37–50.

[25] Us Nuclear Regulatory Commission, Final Safety Evaluation Report Related to Certification of the AP1000 Standard Design, Chapter 22 - Regulatory Treatment of Non-safety Systems, 2004. NUREG-1793.

[26] J. Kang, S. Im, J. Cheon, B. Yun, A parametric study of steam-air mixture condensation on a vertical tube under natural circulation condition, in: 10th International Conference on Boiling and Condensation Heat Transfer (ICBCHT10), Nagasaki, Japan, March 12 - 15, 2018.

[27] J.-W. Yoo, U.-K. Kim, Y.-J. Jang, Y.-G. Lee, An experimental investigation on the external condensation for a vertical tube under forced convection, in: Korean Nuclear Society Spring Meeting, Jeju, Korea, May 17-18, 2018.